

# Accepted Manuscript



Biofilm formation and cellulose expression by *Bordetella avium* 197N, the causative agent of bordetellosis in birds and an opportunistic respiratory pathogen in humans

Kimberley McLaughlin, Ayorinde O. Folorunso, Yusuf Y. Deeni, Dona Foster, Oksana Gorbatiuk, Simona M. Hapca, Corinna Immoor, Anna Koza, Ibrahim U. Mohammed, Olena Moshynets, Sergii Rogalsky, Kamil Zawadzki, Andrew J. Spiers

PII: S0923-2508(17)30017-7

DOI: [10.1016/j.resmic.2017.01.002](https://doi.org/10.1016/j.resmic.2017.01.002)

Reference: RESMIC 3563

To appear in: *Research in Microbiology*

Received Date: 17 November 2016

Revised Date: 16 January 2017

Accepted Date: 16 January 2017

Please cite this article as: K. McLaughlin, A.O. Folorunso, Y.Y. Deeni, D. Foster, O. Gorbatiuk, S.M. Hapca, C. Immoor, A. Koza, I.U. Mohammed, O. Moshynets, S. Rogalsky, K. Zawadzki, A.J. Spiers, Biofilm formation and cellulose expression by *Bordetella avium* 197N, the causative agent of bordetellosis in birds and an opportunistic respiratory pathogen in humans, *Research in Microbiology* (2017), doi: 10.1016/j.resmic.2017.01.002.

This is a PDF file of an unedited manuscript that has been accepted for publication. As a service to our customers we are providing this early version of the manuscript. The manuscript will undergo copyediting, typesetting, and review of the resulting proof before it is published in its final form. Please note that during the production process errors may be discovered which could affect the content, and all legal disclaimers that apply to the journal pertain.

For Publication

**Biofilm formation and cellulose expression by *Bordetella avium* 197N,  
the causative agent of bordetellosis in birds and an opportunistic  
respiratory pathogen in humans**

Kimberley McLaughlin<sup>a\*</sup>, Ayorinde O. Folorunso<sup>a\*\*\*</sup>, Yusuf Y. Deeni<sup>a</sup>, Dona Foster<sup>b</sup>,  
Oksana Gorbatiuk<sup>c</sup>, Simona M. Hapca<sup>a</sup>, Corinna Immoor<sup>a</sup>, Anna Koza<sup>a,\*\*</sup>, Ibrahim U.  
Mohammed<sup>a</sup>, Olena Moshynets<sup>c</sup>, Sergii Rogalsky<sup>d</sup>, Kamil Zawadzki<sup>a</sup>, Andrew J. Spiers<sup>a\*</sup>

<sup>a</sup> *School of Engineering and Technology, Abertay University, Bell Street, Dundee DD1 1HG, UK*

<sup>b</sup> *Department of Biological and Life Sciences, Oxford Brookes University, Gipsy Lane,  
Headington, Oxford OX3 0BP, UK*

<sup>c</sup> *Institute of Molecular Biology and Genetics of the National Academy of Sciences of Ukraine,  
150 Zabolotnoho Street, Kiev 03680, Ukraine*

<sup>d</sup> *Institute of Bioorganic Chemistry and Petrochemistry of the National Academy of Sciences of  
Ukraine, 50 Kharkivske Schose, Kiev 02160, Ukraine*

\*Correspondence : [a.spiers@abertay.ac.uk](mailto:a.spiers@abertay.ac.uk)

\*\*Current address : Technical University of Denmark, Novo Nordisk Foundation Center for Biosustainability, Kemitorvet,  
Building 220, 2800 Kgs. Lyngby, Denmark

\*\*\* Contributed equally to this work

23

24 **Abstract**

25 Although bacterial cellulose synthase (*bcs*) operons are widespread within the  
26 *Proteobacteria* phylum, subunits required for the partial-acetylation of the polymer appear  
27 to be restricted to a few  $\gamma$ -group soil, plant-associated and phytopathogenic  
28 pseudomonads, including *Pseudomonas fluorescens* SBW25 and several *Pseudomonas*  
29 *syringae* pathovars. However, a *bcs* operon with acetylation subunits has also been  
30 annotated in the unrelated  $\beta$ -group respiratory pathogen, *Bordetella avium* 197N. Our  
31 comparison of subunit protein sequences and GC content analyses confirms the close  
32 similarity between the *B. avium* 197N and pseudomonad operons and suggests that, in  
33 both cases, the cellulose synthase and acetylation subunits were acquired as a single unit.  
34 Using static liquid microcosms, we can confirm that *B. avium* 197N expresses low levels of  
35 cellulose in air-liquid interface biofilms and that biofilm strength and attachment levels  
36 could be increased by elevating *c-di*-GMP levels like the pseudomonads, but cellulose was  
37 not required for biofilm formation itself. The finding that *B. avium* 197N is capable of  
38 producing cellulose from a highly-conserved, but relatively uncommon *bcs* operon raises  
39 the question of what functional role this modified polymer plays during the infection of the  
40 upper respiratory tract or survival between hosts, and what environmental signals control  
41 its production.

42

43 **Keywords:** Air-liquid interface; Biofilm; *Bordetella avium*; *c-di*-GMP; Cellulose; Microcosm

44

45 **1. Introduction**

46 *Bordetella avium* is the causative agent of bordetellosis (tracheobronchitis), a highly  
47 contagious upper respiratory disease of domesticated and wild birds [1 - 3], as well an  
48 opportunistic human pathogen that may also be associated with cystic fibrosis [4 - 6]. It is  
49 phylogenetically distinct from *B. bronchiseptica*, *B. parapertussis*, and *B. pertussis*, which  
50 are respiratory pathogens of mammals, though *B. avium* expresses similar virulence  
51 factors and also produces biofilms. However, whilst *Bordetella* polysaccharide (Bps) has  
52 been identified as the primary matrix component in *B. bronchiseptica* RB50 and *B.*  
53 *pertussis* 536 biofilms [7, 8], it has not been reported for *B. avium* biofilms, nor has a *bps*-  
54 like operon been found in the genome of the virulent turkey isolate *B. avium* 197N [9 - 11].  
55 This raises the question of what extracellular polymeric substance (EPS) or substances  
56 are used as the biofilm matrix during host infection or colonisation of other environments  
57 during transmission between hosts.

58 We have noted that the *B. avium* 197N genome [11] has been annotated with a  
59 potential bacterial cellulose synthase (*bcs*) operon (genes BAV2632 – 2623) (Fig. 1). *Bcs*  
60 operons have been identified in the genomes of a wide range of *Proteobacteria*, but  
61 cellulose expression per se has been reported for relatively few strains, including human  
62 gastrointestinal commensals and pathogens, and soil and plant-associated pseudomonads  
63 [12 - 14]. Although the functional role and fitness value of cellulose is poorly understood  
64 [13 - 15], it is associated with biofilm formation in the intestinal epithelium and invasion of  
65 epithelial cells and macrophages [14], and provides a fitness advantage in soils and plant  
66 environments where it may help reduce water stress [16 - 19]. More generally, cellulose  
67 may promote survival in natural environments during transmission between hosts [12].

68 We are interested in determining whether *B. avium* 197N is capable of expressing  
69 cellulose as part of a greater understanding of the functional role of cellulose in a range of  
70 environments and life strategies. Unusually, the *B. avium* 197N *bcs* operon subunits show  
71 close amino acid sequence homology with those found in pseudomonads, particularly the  
72 soil and plant-associated *P. fluorescens* SBW25 (annotated as *wssA-J*, PFLU0300 – 0309  
73 [20], Fig. 1), despite the fact that the *Bordetellae* and *Pseudomonas* are distantly related  
74 genera.

75 The *B. avium* 197N and *P. fluorescens* SBW25 *bcs* operons are further linked by  
76 the inclusion of cellulose acetylation-associated subunits originally described for  
77 *P. fluorescens* SBW25 (*WssF-I*), which affects colony morphology and air-liquid (A-L)  
78 interface biofilms that develop in static microcosms [20, 21]. These subunits are rarely  
79 seen, but are present in a number of plant pathogens, including *P. syringae* pv. *tomato*  
80 DC3000, but not, for example, the closely-related soil-associated *P. putida* KT2440 [13,  
81 21, 22] (Fig. 1). Cellulose is also expressed by *P. putida* KT2400 and *P. syringae* DC3000  
82 in similar conditions [19, 23], and static microcosms have been used to investigate biofilm-  
83 formation more widely amongst the pseudomonads [23, 24] where biofilms can be  
84 quantitatively measured by combined growth, strength and attachment assays [24, 25].

85 *B. avium* 197N has also been reported to produce limited biofilms at the meniscus  
86 of static liquids [26, 27]. We therefore decided to use a static microcosm approach to  
87 characterise *B. avium* 197N biofilm formation more fully under a range of growth  
88 conditions. Although low levels of cellulose expression was observed in wild-type *B. avium*  
89 197N biofilm samples and colonies, we constructed a cellulose-deficient (CD) mutant to  
90 demonstrate that cellulose was not an essential matrix component for biofilm-formation,  
91 suggesting that *B. avium* 197N utilises another but unidentified EPS for this purpose.

## 2. Materials and methods

### 2.1 .Bioinformatics

Bacterial cellulose synthase subunit homologues were identified in *Proteobacteria* complete genomes using NCBI TBLASTN and *P.fluorescens* SBW25 WssA – J protein query sequences (Accession numbers AAL71841 – AAL71850) following the selection criteria described in the Supplementary Methods. A WspR homologue was identified in the *B. avium* 197N genome using *P.fluorescens* SBW25 WspR (AAL71852). Phylogenetic trees were produced using the NCBI COBALT multiple sequence alignment tool and the Neighbour Joining (NJ) method (see Suppl. Methods). Gene and whole genomic GC content data were obtained from the *Pseudomonas* Genome Database ([www.pseudomonas.com](http://www.pseudomonas.com)) and NCBI Genbank. DNA dot plots were produced using the YASS Genomic Similarity Search Tool ([bioinfo.lifl.fr](http://bioinfo.lifl.fr)).

### 2.2. Bacteria and plasmids

Bacteria and plasmids used in this work are listed in Table 1. All strains were kept at -80°C for long-term storage, and stocks produced by adding 15% (v/v) glycerol to overnight cultures. *B. avium* 197N was acquired directly from the American Type Culture Collection (ATCC BAA-1003). Antibiotic susceptibility was assessed using antibiotic disks (MAST, UK). Kanamycin (Km) sensitivity [10] was confirmed using LB plates containing 100 µg.ml<sup>-1</sup> Km incubated at 28°C for 48 hr.

### 2.3. Culturing conditions

Bacteria were cultured at 20, 28, 37, and 42°C using Brain Heart Infusion (BHI; Oxoid, UK), King's B (KB; 20 g proteose peptone No. 3 (BD Biosciences, UK), 10 g glycerol, 5 g K<sub>2</sub>HPO<sub>4</sub>, 1.5 g MgSO<sub>4</sub> per litre) and Luria-Bertani (LB; 10 g NaCl, 10 g

118 tryptone (Oxoid), and 5 g yeast extract (Merck, UK) per litre) media with 1.5% (w/v) Agar  
119 Technical (Oxoid) for plates and antibiotics added as required. Overnight shaken cultures  
120 were used to provide inocula for experiments. Microcosms were 30 ml glass tubes  
121 containing 6 ml growth media [23]. Swimming motility was assessed using soft-agar LB  
122 plates (see Suppl. Methods).

123

#### 124 *2.4. Biofilm formation in static microcosms*

125 Microcosms inoculated with 100  $\mu$ l aliquots of culture and incubated statically were  
126 inspected daily for up to 5 days for signs of A-L interface biofilm-formation, and then by  
127 pouring out into Petri dishes to assess strength and attachment [23]. Biofilms were  
128 quantitatively characterised using the combined biofilm assay in which replicate  
129 microcosms ( $n = 8$ ) were tested for biofilm strength (grams) using small glass balls, biofilm  
130 attachment to the tube walls by staining with crystal violet ( $A_{570}$ ) and total growth by  $OD_{600}$   
131 measurements [24, 25]. These assays were conducted for a number of strains, media and  
132 temperatures, and data sets analysed using a General Linear Model (GLM) approach.

133

#### 134 *2.5. Cellulose expression*

135 Cellulose was assessed using Congo red plates and by fluorescent microscopy.  
136 Congo red plates were BHI, KB, and LB (without NaCl) plus 0.001% (w/v) Congo red [21],  
137 and were drop-inoculated with 5  $\mu$ l aliquots of culture and incubated for 2 – 3 days. Images  
138 were taken using a Nikon D3200 DSLR camera. Samples of colonies and biofilm material  
139 were stained with 10  $\mu$ g.ml<sup>-1</sup> calcofluor for 1 h before viewing at 10x – 40x magnification  
140 using a Leica DMR fluorescent microscope and imaging with an AxioCam MRc digital  
141 camera [21, 28]. Semi-purified biofilm matrix samples were investigated by ELISA using a  
142 cellulose binding domain-containing (SPA-CBD) fusion protein [29] as described in the

143 Suppl. methods. Biofilm samples were also investigated by Fourier transform infrared  
144 spectroscopy (FTIR) and visualised by scanning electron microscopy (SEM) (see Suppl.  
145 methods).

146

## 147 2.6. Construction of pAS296 and the cellulose-deficient (CD) mutant

148 The suicide plasmid pAS296 was designed to disrupt *bcs* operons by homologous  
149 recombination of a *P. fluorescens* SBW25 mini-transposon *wssB::IS- $\Omega$ -Km/hah* (Km<sup>R</sup>)  
150 cassette (the insertion is located 1,693 bp from the start of the 2,219 bp *wssB* gene). This  
151 was integrated into the *B. avium* 197N chromosome following kanamycin selection to  
152 produce the cellulose-deficient (CD) mutant (see Suppl. methods).

153

## 154 2.7. Statistical analyses and modelling

155 Quantitative assays were undertaken with replicates, and means with standard  
156 errors (SE) are shown where appropriate. Data were analysed using JMP v12 (SAS  
157 Institute Inc., USA) statistical software. A general linear model (GLM) approach was used  
158 to investigate the significance of strain, test media, growth and attachment (effects) on  
159 biofilm strength (response) using the combined biofilm assay dataset. Attachment levels  
160 were also modelled as response. Significant effects were examined by LSMeans  
161 Differences Student's t-test and Tukey HSD tests, and associations examined by pairwise  
162 correlations. Differences between means were also tested by ANOVA, t-tests and Turkey-  
163 Kramer HSD tests.

164

## 165 3. Results and discussion

### 166 3.1. Bacterial cellulose synthase (*bcs*) operons within the Proteobacteria.



167 We identified over 100 bacterial whole genome sequences likely to contain fully  
168 functional *bcs* operons based on amino acid sequence homologies to the core cellulose  
169 synthase subunits of *P. fluorescens* SBW25 (Fig. 1 and data not shown), and it is  
170 noteworthy that such a poorly reported or tested phenotype such as the ability to express  
171 cellulose is so commonly annotated amongst the *Proteobacteria*. Within this phylum,  
172 species from one  $\alpha$ -group, two  $\beta$ -group and ten  $\gamma$ -group genera were found to have  
173 convincing *bcs* operons (see Suppl. Table S1). As expected, the organisation of these  
174 operons, in terms of gene order and orientation, was highly variable [14], though  
175 phylogenetic-based clustering at the genus or family levels was seen in Neighbour-Joining  
176 (NJ) trees constructed using core subunit sequences. An example of one NJ tree  
177 generated using WssB homologues (see Suppl. Table S2) and rooted using  $\alpha$ -group  
178 *Proteobacteria* is given in Fig. 2. The phylogenetic-based clustering of homologues seen  
179 here suggests that most sequence variation in core subunits is probably acquired through  
180 vertical transmission. However, the close branching of distantly related genera such as the  
181 *Bordetellae* and *Pseudomonas* in these trees suggests that *bcs* operons may have been  
182 horizontally transmitted at an early stage in the radiation of the *Proteobacteria*.

183 We note the increasing number of plant pathogens including *Burkholderia* ( $\beta$ -  
184 group), *Dickeya*, and *Pseudomonas* ( $\gamma$ -group) spp., and animal pathogens including  
185 *Bordetella* ( $\beta$ -group), *Escherichia*, *Klebsiella*, *Salmonella* and *Shigella* ( $\gamma$ -group) spp.,  
186 encode *bcs* operons and are likely to express cellulose (Suppl. Table S1). Although these  
187 pathogens have diverse hosts and survive in a wide range of environments, cellulose  
188 might play a common role in single cell attachment, microcolony and biofilm formation, and  
189 protection against predation, disturbance or stress [13, 14].

### 191 3.2. The *bcs* operon in *B. avium* 197N

192 Following our survey of *bcs* operons within the *Proteobacteria*, we shifted our  
193 attention to the operon annotated in the *B. avium* 197N genome. The link between this  
194 avian and opportunistic human respiratory pathogen [9 - 11] and the soil- and plant-  
195 associated pseudomonads is intriguing, because of the high levels of *bcs* subunit  
196 homology with *P. fluorescens* SBW25 and the presence of the rarely seen cellulose  
197 acetylation-associated subunits apparently restricted to *P. fluorescens* SBW25 and a  
198 number of related plant pathogens, including *P. syringae* DC3000 [21, 22].

199 The *B. avium* 197N *bcs* operon is also notable, as in NJ trees, the WssBCDE  
200 homologues from *B. avium* 197N, *P. fluorescens* SBW25 and *P. syringae* DC3000 were  
201 always clustered together, but distant from the *P. putida* KT2400 homologues (see also  
202 [22]). A representative NJ tree for WssB homologues is shown in Fig. 2 and a comparison  
203 of WssA – I homologues provided in Table 2.

204 However, the *B. avium* 197N *bcs* operon differs significantly from the *P. fluorescens*  
205 SBW25, *P. putida* KT2400 and *P. syringae* DC3000 operons by the duplication of WssC  
206 (annotated as WssC1 and WssC2), which challenges our presumption that this bacterium  
207 could express cellulose. Although the duplication is apparent in an alignment of the *B.*  
208 *avium* 197N and *P. fluorescens* SBW25 genomic sequences, WssC1 and WssC2 are not  
209 direct copies of one another and share only 47% identity at the protein level (97%  
210 coverage, 0.0 E value) (see Suppl. Fig. S1). Furthermore, WssC1 and WssC2 branch  
211 separately in a NJ tree containing *P. fluorescens* SBW25, *P. putida* KT2400 and *P. syringae*  
212 DC3000 WssC homologues (Suppl. Fig. S1). The alignment of *B. avium* 197N and  
213 *P. fluorescens* SBW25 sequences also indicates that the two genomes do not share  
214 significant levels of homology beyond the boundaries of the *bcs* operons, suggesting that  
215 one or the other acquired the operon by a limited lateral gene transfer event.

216 A comparison of the GC content of the *bcs* genes indicates that the *B. avium* 197N,  
217 *P. fluorescens* SBW25, *P. putida* KT2400 and *P. syringae* DC3000 operons are more  
218 similar to one another than they are to the *P. putida* KT2400 operon ( $\alpha = 0.05$ ) (Fig. 3). The  
219 mean GC contents of the *bcs* genes of *P. fluorescens* SBW25, *P. putida* KT2400 and  
220 *P. syringae* DC3000 were also significantly different from their whole genome GC content  
221 ( $p \leq 0.0003$ ), suggesting that these bacteria had acquired the *bcs* operons relatively  
222 recently and before much amelioration of divergent sequences could occur. In contrast, no  
223 significant difference was observed between the *B. avium* 197N *bcs* genes and whole  
224 genome GC content ( $p = 0.2033$ ), suggesting that the transfer event occurred much earlier  
225 in this bacterium or that the ancestral *bcs* donor was more similar to the *Bordetellae* than  
226 to the pseudomonads. As the GC content of intergenic regions and coding sequences are  
227 frequently correlated in bacterial genomes [30], a direct comparison between the GC  
228 content of the *bcs* genes with the GC content of all other chromosomally encoded genes is  
229 unlikely to produce a substantially different result. However, we have not yet investigated  
230 the regions surrounding each of the *bcs* operons, which may show significant differences  
231 from the rest of the chromosomes.

232 Finally, no significant differences were observed between the GC content of core  
233 synthase and acetylation-associated genes within operons ( $p \geq 0.5085$ ), and no significant  
234 correlations found between GC content and gene order ( $p > 0.05$ ). This suggests that the  
235 acetylation-associated genes had been transferred and maintained with the core synthase  
236 genes, rather than as subsequent and independently acquired functions.

### 237 238 3.3. *B. avium* 197N biofilm formation in static microcosms

239 Given the close protein homologies and conserved operon structures seen between  
240 the *B. avium* 197N *bcs* operon and the *P. fluorescens* SBW25, *P. putida* KT2400 and

241 *P.syringae* DC3000 *bcs* operons, we were interested in determining whether *B. avium*  
242 197N expressed cellulose despite the WssC duplication, and whether it also played a role  
243 in A-L interface biofilm formation, as it does for some pseudomonads. As *B. avium* 197N  
244 has been reported to form limited biofilms at the meniscus of static liquids [26, 27], we  
245 decided to use the static microcosm approach we had previously developed to investigate  
246 A-L interface biofilm formation by *P.fluorescens* SBW25 and other pseudomonads [13, 23,  
247 24]. In these, competition for O<sub>2</sub> which is otherwise growth-limiting in the liquid column  
248 drives biofilm formation at the liquid surface [31], even in the absence of host-derived  
249 factors or environmental signals that might normally regulate such activity, including the  
250 expression of biofilm-associated EPS.

251 In order to determine whether *B. avium* 197N could form biofilms in static  
252 microcosms, a range of media and incubation temperatures (BHI, KB and LB; 20 – 42°C)  
253 were tested, as although *B. avium* 197N is routinely grown in BHI at 37°C, phenotypic  
254 differences have been noted under other conditions [9, 10, 32, 33]. We found clear visual  
255 evidence of growth (i.e. culture turbidity) and A-L interface biofilm formation, including  
256 culture turbidity, films extending across the A-L interface and sunken debris within three  
257 days of incubation under all conditions tested (Fig. 4). The biofilms formed in KB  
258 microcosms were particularly obvious and robust, and were characterised as physically  
259 cohesive (PC)-class / air-liquid-solid surface (A-L-S) interface-type biofilms [23, 24]. In  
260 contrast, BHI biofilms were almost transparent with white flecks of material, and LB  
261 biofilms were very thin and fragile.

262 We recovered biofilm material from microcosms and spread it onto plates to  
263 investigate colony morphologies. In *P.fluorescens* SBW25 populations, radiation (i.e.  
264 mutation) results in significant numbers of biofilm-forming “wrinkly spreaders” (WSs)  
265 identifiable by an altered colony morphology [34]. However, only wild-type colony

266 morphologies were observed from 3 day-old *B. avium* 197N biofilm samples, and no other  
267 signs of radiation were seen in KB microcosms incubated for up to 15 days (e.g. in  
268 siderophore production, colouration, motility, etc.). This suggests that the biofilm formation  
269 we observed in experimental static microcosms is the result of a normal physiological  
270 response by *B. avium* 197N, rather than the activity of biofilm-producing mutants. Further  
271 testing using modified media containing avian tissue-derived signal compounds, cell  
272 cultures, tracheal rings or lung tissue will be required to determine whether biofilm  
273 formation is a behaviour more specifically associated with host infection or the colonisation  
274 of water, plants, and soils during transmission between hosts.

#### 275 276 3.4. Quantitative characterisation of the *B. avium* 197N biofilm

277 In order to place *B. avium* 197N A-L interface biofilm formation in static microcosms  
278 into context, we compared *B. avium* 197N with wild-type *P. fluorescens* SBW25 and the  
279 *P. fluorescens* SBW25 WS mutant using a range of media and a quantitative combined  
280 biofilm assay measuring microcosm growth, biofilm strength and attachment levels [24].  
281 Wild-type *P. fluorescens* SBW25 was included, as it produces a poorly attached, fragile  
282 biofilm referred to as the VM biofilm [35], whilst the WS produces a robust, well-attached  
283 biofilm in KB microcosms [20, 21, 28, 34].

284 We modelled biofilm strength using a GLM approach, and both strain and medium  
285 were found to be significant ( $p \leq 0.0001$ , see Suppl. Table S3, Model 1); representative  
286 data for KB microcosms are shown in Fig. 5. Although the VM and WS biofilms were  
287 significantly different from one another, the *B. avium* 197N biofilms were of intermediate  
288 strength (Fig. 5B) and could not be differentiated from either the VM or WS biofilms ( $\alpha =$   
289 0.05). The strongest *B. avium* 197N biofilms were produced in KB microcosms, and across  
290 all three strains, KB biofilms could be differentiated from BHI and LB biofilms ( $\alpha = 0.05$ )

291 which suggests that biofilm formation was influenced by media composition. Overall  
292 growth and biofilm attachment levels were not found to have significant effects on biofilm  
293 strength ( $p > 0.05$ ) across the three strains tested in these microcosms. However, in  
294 previous work, the VM biofilm has been shown to have significantly lower attachment  
295 levels than the WS biofilm [35]. Finally, we also modelled biofilm attachment levels, as  
296 biomass at the meniscus is often used as a measure of biofilm growth in microtitre plate-  
297 based assays [36]. In this, the strain effect was found to be weakly insignificant ( $p =$   
298  $0.0501$ , Suppl. Table S3, Model 2), with the *B. avium* 197N biofilm differentiated from the  
299 VM biofilm, but neither from the WS biofilm ( $\alpha = 0.05$ ).

### 301 3.5. Cellulose expression by *B. avium* 197N

302 We used the cellulose-binding dye calcofluor and fluorescent microscopy to  
303 demonstrate that cellulose fibres were present in *B. avium* 197N colonies and biofilm  
304 samples (Fig. 6A). However, relatively little cellulose was observed compared to that  
305 reported for VM and WS biofilms [21, 35], and none was observed in samples from a  
306 cellulose-deficient (CD) mutant we produced by disrupting the *B. avium* 197N *bcs* operon  
307 with a *P. fluorescens* SBW25 *wssB::IS- $\Omega$ -Km/hah* cassette. Additional evidence to support  
308 the presence of cellulose at low levels in biofilms was obtained by ELISA using a cellulose  
309 binding-domain-containing (SPA-CBD) fusion protein [29]. This showed a 2.5x increase in  
310 cellulose levels in semi-purified biofilm matrix samples compared to the CD  
311 mutant, though this assay was unreplicated and may need further testing. However,  
312 cellulose levels were insufficient for detection by FTIR (see Suppl. Fig. S2). Despite this,  
313 significant differences in biofilm strength and attachment levels were found between the *B.*  
314 *avium* 197N and CD mutant biofilms ( $\alpha = 0.05$ ) (Fig. 5). These changes may not  
315 necessarily be due to the loss of cellulose in the biofilm per se, but might result from the

316 loss of the cellulose synthase complex which effects other regulatory systems involved in  
317 the expression of biofilm matrix components and attachment factors.

318 We suggest that the low levels of cellulose seen in *B. avium* 197N biofilms  
319 produced under the conditions tested here may be the result of either the unusual *wssC*  
320 duplication, which might reduce *wss* operon transcription or cellulose synthase complex  
321 assembly, or the result of leaky transcriptional or synthase regulation in the absence of the  
322 normal signals required to express cellulose. It is possible that host-specific factors are  
323 required to induce cellulose expression to higher levels during invasion of avian tissues, or  
324 that other environmental signals are required for expression during transmission between  
325 hosts for survival in water, soils or plants. Future analysis will require transcriptional  
326 analyses of the *wss* operon, plus quantitative measurements of cellulose production, to  
327 better understand how and when cellulose production is controlled by this bacterium.

328 It remains unclear what EPS is being utilised by *B. avium* 197N as the primary  
329 biofilm matrix in these microcosms, as *B. avium* 197N lacks a *bps*-like operon required to  
330 express the Bps polymer produced by other *Bordetellae* [7, 8, 11]. SEM imaging of wild-  
331 type *B. avium* 197N and CD mutant biofilm samples appear very similar (Fig. 6B) and are  
332 like those produced by *B. bronchiseptica* RB50 and *B. pertussis* Bp536, for which Bps is  
333 required for biofilm formation [26, 27]. *B. avium* 197N biofilms may utilise a similar  
334 polysaccharide, eDNA or a proteinaceous attachment factor or adhesin as the primary  
335 biofilm matrix component, but further biochemical and genetic analyses will be required to  
336 identify the nature of this EPS.

### 337 338 3.6. Involvement of *ci-di-GMP* in *B. avium* 197N in colony morphology and biofilms

339 Biofilm formation and cellulose expression in *P. fluorescens* SBW25 is primarily  
340 controlled by *c-di-GMP* levels regulated by WspR and other diguanylate cyclases (DGCs)

[34]. DGCs are found in other pseudomonads and *Bordetellae*, and we have noted a close homologue in *B. avium* 197N (WP\_012416712; 336 aa, with 63% ID and an E value of 1e-149). In order to determine whether *c-di*-GMP levels may also play a role in *B. avium* 197N biofilm formation or cellulose expression, we tested the effect of overexpression of a constitutively active and dominant WspR19 mutant that induces a phenotype indistinguishable from the WS in *P. fluorescens* SBW25 [28, 37]. As WspR19 is functional in other pseudomonads and in more distantly related bacteria such as *Caulobacter crescentus* CB15 [23, 38, 39], it might also have an impact on the phenotype of *B. avium* 197N regardless of the activity of WP\_012416712.

We first tested whether WspR19 affected *B. avium* 197N swimming motility [10], as the expression of a similar DGC in *B. bronchiseptica* 9.73 was found to repress swimming motility through the elevation of *c-di*-GMP levels [40]. WspR19 was found to partially repress swimming to 11 – 18%% of the levels shown by *B. avium* 197N carrying the control plasmid ( $p \leq 0.0001$ ). We then investigated whether WspR and WspR mutants affected colony morphology, including the uptake of Congo red stain used to assess cellulose and attachment factor expression [20, 21, 28, 35]. WspR19 was found to have a consistent impact on *B. avium* 197N colony morphology, resulting in larger and slightly rougher colonies with higher levels of Congo red staining compared to wild-type *B. avium* 197N and the CD mutant (Fig. 6C). In comparison, *B. avium* 197N colonies expressing the wild-type WspR protein (WspR12) [28, 41] were only slightly stained by Congo red, and colonies expressing the dominant-negative WspR9 mutant [41] were indistinguishable from *B. avium* 197N, the CD mutant and the plasmid control colonies. Although more cellulose could be observed by fluorescent microscopy in colony material produced by *B. avium* 197N expressing WspR19 compared to either *B. avium* 197N with the control plasmid or the CD mutant (data not shown), it is unclear whether the changes in colony



366 morphology are the result of minor increases in cellulose levels or changes in other EPS or  
367 attachment factors which also bind Congo red.

368 The expression of WspR mutants in *B. avium* 197N also affected biofilm strength,  
369 with strain, medium and growth all found to have significant effects ( $p \leq 0.0001$ , Suppl.  
370 Table S3, Model 3). In particular, strains could be differentiated into three groups, with *B.*  
371 *avium* 197N carrying the control plasmid or expressing WspR9 having the least effect on  
372 strength, WspR12 having an intermediate effect, and WspR19 having the greatest effect  
373 on strength ( $\alpha = 0.05$ ). The strongest biofilms were produced in KB microcosms by *B.*  
374 *avium* 197N expressing WspR19 which were significantly stronger than the plasmid control  
375 (2.5 x,  $p = 0.0353$ ), though growth was significantly reduced (0.6 x,  $p = 0.0002$ ). This  
376 suggests that WspR19 has a negative pleiotropic effect when expressed in *B. avium* 197N,  
377 as it does in *P. fluorescens* SBW25 [37]. Although the strain was weakly insignificant ( $p <$   
378  $0.0727$ ) when attachment was modelled (Suppl. Table S3, Model 4), it seems likely that  
379 biofilm formation by *B. avium* 197N in static microcosms under the conditions tested here  
380 is regulated to some degree by *c-di*-GMP levels.

381 In conclusion, bacterial cellulose synthase *bcs* operons are common amongst the  
382 *Proteobacteria*, though acetylation-associated genes are rare and have only been  
383 identified in a select group of pseudomonads and a few other species including *B. avium*  
384 197N. In this work, we confirm that *B. avium* 197N is able to express cellulose at low  
385 levels, though it was not necessary for the formation of A-L interface biofilms in static  
386 microcosms, and further investigation is required to identify the primary matrix components  
387 utilised by *B. avium* 197N under the conditions tested here and to identify the  
388 environmental signals and regulatory mechanisms which control expression under natural  
389 conditions. Although cellulose might be used during infection of the upper respiratory  
390 tract of hosts, it may also be important for survival between hosts in water, soil or on plant

391 surfaces, and this might explain why *bcs* operons are carried by environmental bacteria as  
392 well as pathogenic and commensal intestinal bacteria.

### 394 **Conflict of interests**

395 The authors declare that there is no conflict of interests regarding the publication of  
396 this paper.

### 398 **Author's contributions**

399 KMcL and AOF contributed equally to this work as first co-authors. KMcL, OM and  
400 AJS designed the experiments. AOF, KZ, DF and AJS carried out the bioinformatics  
401 analyses. KMcL, CI, AK, IUM, OM and SR carried out the experiments. KMcL, SMH and  
402 AJS analysed the data. AJS and OM prepared the manuscript with comments from all  
403 authors. AJS, YD and OM were responsible for the management of this project, with AJS  
404 leading.

### 406 **Supplementary material**

407 **Methods:** Construction of pAS296 and the cellulose-deficient (CD) mutant; Fourier  
408 transform infrared spectroscopy (FTIR); plasmid isolation, electroporation and  
409 strain manipulation; scanning electron microscopy (SEM); and swimming  
410 motility.

411 **Fig. S1.** The *B. avium* 197N *bcs* operon shows DNA level similarities with those found  
412 in key pseudomonads.

413 **Fig. S2.** FTIR does not differentiate between wild-type *B. avium* 197N and cellulose-  
414 deficient (CD) mutant biofilm samples.

415 **Table S1.** *Proteobacteria* having convincing bacterial cellulose synthase (*bcs*) operons.

416 **Table S2.** Representative *Proteobacteria* having WssB homologues.

417 **Table S3.** General linear modelling of biofilm strength and attachment levels.

418

419 **References**

- 420 1. Hinz KH, Glünder G. Occurrence of *Bordetella avium* sp. nov. and *Bordetella*  
421 *bronchiseptica* in birds. [In German]. Berl Munch Tierarztl Wochenschr 1985;98:369-  
422 73.
- 423 2. Raffel TR, Register KB, Marks SA, Temple L. Prevalence of *Bordetella avium*  
424 infection in selected wild and domesticated birds in the eastern USA. J Wildl Dis  
425 2002;38:40-46.
- 426 3. Grespan A, Camera O, Knöbl T, Gomes CR, Felizardo MR, Ferreira TSP, et al.  
427 Virulence and molecular aspects of *Bordetella avium* isolated from cockatiel chicks  
428 (*Nymphicus hollandicus*) in Brazil. Vet Microbiol 2012;160:530-34.
- 429 4. Spilker T, Liwienski AA, LiPuma JJ. Identification of *Bordetella* spp. in respiratory  
430 specimens from individuals with cystic fibrosis. Clin Microbiol Infect 2008;14:504-6.
- 431 5. Harrington AT, Castellanos JA, Ziedalski TM, Clarridge JE, Cookson BT. Isolation of  
432 *Bordetella avium* and novel *Bordetella* strain from patients with respiratory disease.  
433 Emerg Infect Dis 2009;15:72-4.
- 434 6. Bos AC, Beemsterboer P, Wolfs TFW, Versteegh FGA, Arets HGM. *Bordetella*  
435 species in children with cystic fibrosis: what do we know?: The role in acute  
436 exacerbations and chronic course. J Cyst Fibros 2011;10:307-12.
- 437 7. Sloan GP, Love CF, Sukumar N, Mishra M, Deora R. The *Bordetella* Bps  
438 polysaccharide is critical for biofilm development in the mouse respiratory tract. J  
439 Bacteriol 2007;189:8270-82.
- 440 8. Conover MS, Sloan GP, Love CF, Sukumar N, Deora R. The Bps polysaccharide of  
441 *Bordetella pertussis* promotes colonization and biofilm formation in the nose by  
442 functioning as an adhesion. Mol Microbiol 2010;77:1439-55.

- 443 9. Gentry-Weeks CR, Cookson BT, Goldman WE, Rimler RB, Porter SB, Curtiss R.  
444 Dermonecrotic toxin and tracheal cytotoxin, putative virulence factors of *Bordetella*  
445 *avium*. Infect Immunol 1988;56:1698-1707.
- 446 10. Temple LA, Weiss AA, Walker KE, Barnes HJ, Christensen VL, Miyamoto DM, et al.  
447 *Bordetella avium* virulence measured *in vivo* and *in vitro*. Infect Immunity  
448 1998;66:5244-51.
- 449 11. Sebahia M, Preston A, Maskell DJ, Kuzmiak H, Connell TD, King ND, et al.  
450 Comparison of the genome sequence of the poultry pathogen *Bordetella avium* with  
451 those of *B. bronchiseptica*, *B. pertussis*, and *B. parapertussis* reveals extensive  
452 diversity in surface structures associated with host interaction. J Bacteriol  
453 2006;188:6002-15.
- 454 12. Römbling U. Molecular biology of cellulose production in bacteria. Res Microbiol  
455 2002;153:205-12.
- 456 13. Spiers AJ, Deeni YY, Folorunso AO, Koza A, Moshynets O, Zawadzki K. Cellulose  
457 expression in *Pseudomonas fluorescens* SBW25 and other environmental  
458 pseudomonads. In: Cellulose. Van De Ven TGM, Godbout L, editors. Rijeka,  
459 Croatia, InTech; 2013.
- 460 14. Römbling U, Galperin MY. Bacterial cellulose biosynthesis: diversity of operons,  
461 subunits, products, and functions. Trends Microbiol 2015; 23:545-57.
- 462 15. Augimeri R, Varley AJ, Strap JL. Establishing a role for bacterial cellulose in  
463 environmental interactions: lessons learned from diverse biofilm-producing  
464 *Proteobacteria*. Front Microbiol 2015;6:1282.
- 465 16. Gal M, Preston GM, Massey RC, Spiers AJ, Rainey PB. Genes encoding a  
466 cellulosic polymer contribute toward the ecological success of *Pseudomonas*  
467 *fluorescens* SBW25 on plant surfaces. Mol Ecol 2003;12:3109-21.

- 468 17. White AP, Gibson DL, Kim W, Kay WW, Surette MG. Thin aggregative fimbriae and  
469 cellulose enhance long-term survival and persistence of *Salmonella*. *J Bacteriol*  
470 2006;188:3219-27.
- 471 18. Gualdi L, Tagliabue L, Bertagnoli S, Ieranò T, De Castro C, Landini P. Cellulose  
472 modulates biofilm formation by counteracting curli-mediated colonization of solid  
473 surfaces in *Escherichia coli*. *Microbiology* 2008; 154:2017-24.
- 474 19. Nielsen L, Li X, Halverson LJ. Cell–cell and cell–surface interactions mediated by  
475 cellulose and a novel exopolysaccharide contribute to *Pseudomonas putida* biofilm  
476 formation and fitness under water-limiting conditions. *Environ Microbiol*  
477 2011;13:1342-56.
- 478 20. Spiers AJ, Kahn SG, Bohannon J, Travisano M, Rainey PB. Adaptive divergence in  
479 experimental populations of *Pseudomonas fluorescens*. I. Genetic and phenotypic  
480 bases of Wrinkly Spreader fitness. *Genetics* 2002;161:33-46.
- 481 21. Spiers AJ, Bohannon B, Gehrig SM, Rainey PB. Biofilm formation at the air–liquid  
482 interface by the *Pseudomonas fluorescens* SBW25 Wrinkly Spreader requires an  
483 acetylated form of cellulose. *Mol Microbiol* 2003;50:15-27.
- 484 22. Arrebola E, Carrión VJ, Gutiérrez-Barranquero JA, Pérez-García A, Rodríguez-  
485 Palenzuela P, Cazorla FM, et al. Cellulose production in *Pseudomonas syringae* pv.  
486 *syringae*: a compromise between epiphytic and pathogenic lifestyles. *FEMS*  
487 *Microbiol Ecol* 2015;91:fiv071.
- 488 23. Ude S, Arnold DL, Moon CD, Timms-Wilson T, Spiers AJ. Biofilm formation and  
489 cellulose expression among diverse environmental *Pseudomonas* isolates. *Environ*  
490 *Microbiol* 2006;8:1997-2011.

- 491 24. Robertson M, Hapca SM, Moshynets O, Spiers AJ. Air-liquid interface biofilm  
492 formation by psychrotrophic pseudomonads recovered from spoilt meat. *Antonie van*  
493 *Leeuwenhoek* 2013;103:251-9.
- 494 25. Udall YC, Deeni Y, Hapca SM, Raikes D, Spiers AJ. The evolution of biofilm-  
495 forming Wrinkly Spreaders in static microcosms and drip-fed columns selects for  
496 subtle differences in wrinkleality and fitness. *FEMS Microbiol Ecol* 2015;91:fiv057.
- 497 26. Mishra M, Parise G, Jackson KD, Wozniak DJ, Deora R. The BvgAS signal  
498 transduction system regulates biofilm development in *Bordetella*. *J Bacteriol*  
499 2005;187:1474-84.
- 500 27. Parise G, Mishra M, Itoh Y, Romeo T, Deora R. Role of a putative polysaccharide  
501 locus in *Bordetella* biofilm development. *J Bacteriol* 2007;198:750-60.
- 502 28. Spiers AJ, Rainey PB. The *Pseudomonas fluorescens* SBW25 Wrinkly Spreader  
503 biofilm requires attachment factor, cellulose fibre and LPS interactions to maintain  
504 strength and integrity. *Microbiology* 2005;151:2829-39.
- 505 29. Gorbatiuk OB, Tsapenko MV, Pavlova MV, Okunev OV, Kordium VA. Bioaffinity  
506 sorbent based on immobilized protein A *Staphylococcus aureus*: development and  
507 application. *Biopolym Cell* 2012;28:141-8.
- 508 30. Brocchieri L. The GC content of bacterial genomes. *J. Phylogen Evolution Biol*  
509 2014; 2:1.
- 510 31. Koza A, Moshynets O, Otten W, Spiers AJ. Environmental modification and niche  
511 construction: developing O<sub>2</sub> gradients drive the evolution of the Wrinkly Spreader.  
512 *ISME J* 2011; 5:665-73.
- 513 32. Loker SB, Temple LM, Preston A. The *Bordetella avium* BAV1965-1962 fimbrial  
514 locus is regulated by temperature and produces fimbriae involved in adherence to  
515 Turkey tracheal tissue. *Infect Immunity* 2011;79:2423-9.

- 516 33. Beach NM, Thompson S, Mutnick R, Brown L, Kettig G, Puffenbarger R, et al.  
517 *Bordetella avium* antibiotic resistance, novel enrichment culture, and antigenic  
518 characterization. *Vet Microbiol* 2012;160:189-96.
- 519 34. Spiers AJ. A mechanistic explanation linking adaptive mutation, niche change and  
520 fitness advantage for the Wrinkly Spreader. *Int J Evolutionary Biol* 2014;Article ID  
521 675432.
- 522 35. Koza A, Hallett PD, Moon CD, Spiers AJ. Characterization of a novel air-liquid  
523 interface biofilm of *Pseudomonas fluorescens* SBW25. *Microbiology* 2009;  
524 155:1397-1406.
- 525 36. O'Toole GA, Kolter R. Initiation of biofilm formation in *Pseudomonas fluorescens*  
526 WCS365 proceeds via multiple, convergent signalling pathways: a genetic analysis.  
527 *Mol Microbiol* 1998;28:449-61.
- 528 37. Goymer P, Kahn SG, Malone JG, Gehrig SM, Spiers AJ, Rainey PB. Adaptive  
529 divergence in experimental populations of *Pseudomonas fluorescens*. II. Role of the  
530 GGDEF regulator WspR in evolution and development of the Wrinkly Spreader  
531 phenotype. *Genetics* 2006; 173:515-26.
- 532 38. D'Argenio DA, Calfee MW, Rainey PB, Everett C, Pesci EC. Autolysis and  
533 autoaggregation in *Pseudomonas aeruginosa* colony morphology mutants. *J*  
534 *Bacteriol* 2002;184:6481-9.
- 535 39. Aldridge P, Paul R, Goymer P, Rainey P, Jenal U. Role of the GGDEF regulator  
536 PleD in polar development of *Caulobacter crescentus*. *Mol Microbiol* 2003;47:1695-  
537 1708.
- 538 40. Sisti F, Ha DG, O'Toole GA, Hozbor D, Fernández J. Cyclic-di-GMP signalling  
539 regulates motility and biofilm formation in *Bordetella bronchiseptica*. *Microbiology*  
540 2013; 159:869-79.

- 541 41. Goymer PJ. The role of the WspR response regulator in the adaptive evolution of  
 542 experimental populations of *Pseudomonas fluorescens* SBW25. D.Phil. thesis.  
 543 Oxford, University of Oxford; 2002.
- 544 42. Rainey PB, Bailey MJ. Physical and genetic map of the *Pseudomonas fluorescens*  
 545 SBW25 chromosome. *Mol Microbiol* 1996;19:521-33.

## 547 Figure Legends

548 Fig. 1. **Bacterial cellulose synthase (*bcs*) operon structures.** *Bcs* operons have  
 549 been identified in the whole-genome sequences of a wide range of bacteria. In  
 550 *P. fluorescens* SBW25 the genes are annotated as *wssA – J* and are predicted  
 551 to form the core cellulose synthase complex (dark blue) including an  
 552 endoglucanase (light blue) and associated acetylation subunits (green), and to  
 553 be involved in the localization of the complex at the periplasmic membrane  
 554 (mauve) (top section). Shown also are the *bcs* operons of *P. putida* KT2400,  
 555 *P. syringae* DC3000 and *B. avium* 197N, which also contains a duplication of a  
 556 truncated version of *wssC* (blue stripes). The scale bar indicates 1 kb.

557

558 Fig. 2. **Phylogenetic analyses of representative WssB homologues.** Shown here is  
 559 a phylogenetic tree showing the relationships between WssB proteins from the  
 560 key strains *B. avium* 197N, *P. fluorescens* SBW25, *P. putida* KT2400 and  
 561 *P. syringae* DC3000 (bold), as well as a number of other bacteria in which *wss*-  
 562 like *bcs* operons have been identified. A number of *Komagataeibacter* spp.  
 563 sequences were used to root the tree (indicated by the black square), and these  
 564  $\alpha$ -group sequences represented by *Gluconacetobacter xylinus* E25 (light blue)  
 565 were found to cluster separately from the other  $\beta$  and  $\gamma$ -group sequences. Most



566  $\gamma$ -group *Pseudomonas* spp. sequences clustered together (light green).

567 Although the  $\beta$ -group sequences root at the base of the *Pseudomonas* spp.

568 cluster, the *Bordetella* spp. sequences including *B. avium* 197N (purple)

569 clustered separately from the *Burkholderia* spp. (light orange). This NJ tree is

570 based on COBALT multiple alignments of the coding sequences listed in Table

571 1. Some sequences have not been labelled in the tree for clarity. The distance

572 bar indicates 0.1 units.

573

574 **Fig. 3. GC content of the *bcs* operons.** An analysis of the *bcs* operons from *B. avium*  
 575 197N, *P. fluorescens* SBW25, *P. putida* KT2400 and *P. syringae* DC3000 reveals  
 576 substantial variation in gene GC content within operons. The GC contents of  
 577 individual genes (grey circles), the mean with SE bars for each operon  
 578 (squares) and each genome (triangles) are shown. See the main results  
 579 section for statistical comparisons.

580

581 **Fig.4. *B. avium* 197N forms biofilms at the air-liquid (A-L) interface of static**  
 582 **microcosms.** Shown are representative images of *B. avium* 197N biofilms *in*  
 583 *situ* in BHI, KB and LB microcosms (A – C, top row) and of biofilm material after  
 584 pouring into petri dishes (bottom row). Biofilms become progressively more  
 585 robust with longer incubation periods, but tend to detach from the meniscus  
 586 region and sink to the bottom of the vials. Microcosms were incubated at 20°C  
 587 for three days before imaging.

588

589 **Fig. 5. The *B. avium* 197N biofilm is intermediate in strength but with high levels**  
 590 **of attachment.** Biofilm formation in static microcosms can be quantified by

591 using a combined biofilm assay in which microcosm growth (A), biofilm strength  
592 (B) and attachment levels (C) are determined. Shown here are data for  
593 *P. fluorescens* SBW25 which produces the VM biofilm (white bars), the WS  
594 which produces the WS biofilm (black), *B. avium* 197N (indicated by 'Wt' for  
595 wild-type, dark grey), and the *B. avium* 197N cellulose-deficient (CD) mutant  
596 (light grey) incubated in KB microcosms at 20°C for three days before assay.  
597 Means and SE are shown. Significant differences between means were  
598 observed for growth ( $p < 0.0001$ ), strength ( $p < 0.0001$ ) and attachment ( $p =$   
599  $0.0005$ ); means within assays not connected by the same letter are significantly  
600 different ( $\alpha = 0.05$ ).

601  
602 **Fig. 6. Cellulose is expressed by *B. avium* 197N but is not essential for biofilms.**

603 Cellulose fibres forming the matrix of the *P. fluorescens* SBW25 WS mutant are  
604 readily visualised by fluorescent microscopy after staining with calcofluor (A). In  
605 comparison, only low levels of cellulose expression can be detected in *B. avium*  
606 197N biofilm samples and none in the cellulose-deficient (CD) mutant even at  
607 higher magnification. Qualitative comparison of scanning electron microscope  
608 images of *B. avium* 197N and CD mutant biofilm samples show no obvious  
609 differences in structure (B), suggesting that the presence of cellulose has little  
610 apparent impact on biofilm structure. Congo red, which also binds cellulose and  
611 other compounds, including proteinaceous attachment factors, stains colonies  
612 of *B. avium* 197N expressing the constitutively active diguanylate cyclase  
613 WspR19 mutant *in trans* (C). However, little staining is apparent in colonies of  
614 wild-type *B. avium* 197N, *B. avium* 197N transformed with pVSP61 (the control  
615 plasmid), pVSP61-WspR9, pVSP61-WspR12 or the CD mutant.

**Table 1.** Bacteria and plasmids.

<i>Strains and plasmids</i>	<i>Comment</i>	<i>Source / Reference</i>
<i>Bordetella avium</i> 197N	Wild-type strain (ATCC BAA-1003), Km <sup>S</sup> , Tc <sup>S</sup> .*	ATCC [9, 10]
<i>Ba.</i> 197N cellulose deficient (CD) mutant	<i>Ba.</i> 197N:: <i>wssB</i> ::IS $\Omega$ -Km/ <i>hah</i> constructed using pAS296, Km <sup>R</sup> .	This work
<i>Escherichia coli</i> K12 DH5 $\alpha$	Standard host for maintaining plasmids.	Gibco-BRL, UK
<i>Pseudomonas fluorescens</i> SBW25	Wild-type strain expressing low-levels of cellulose and producing a weak, viscous mass (VM)-class biofilm.	[42]
<i>Pf.</i> SBW25 Wrinkly Spreader (WS) mutant	<i>Pf.</i> SBW25 <i>wssF</i> ( <i>S301R</i> ) over-expressing cellulose and producing a robust, physically cohesive (PC)-class biofilm.	[20]
pAS296	Suicide plasmid designed to disrupt <i>Pf.</i> SBW25 <i>wss</i> -like <i>bcs</i> operons derived from pNR9.3, Km <sup>R</sup> .	This work
pNR9.3	A self-replicating <i>wssB</i> ::IS $\Omega$ -Km/ <i>hah</i> mini-transposon construct, Km <sup>R</sup> .	S. Giddens
pVSP61-Tc	A modified version of the pVSP61 broad host-range cloning vector, Km <sup>R</sup> and Tc <sup>R</sup> .	[28, 41]
pVSP61-WspR9-Tc	pVSP61-Tc expressing the dominant-negative diguanylate cyclase mutant, WspR9 ( <i>G296R</i> ), Km <sup>R</sup> and Tc <sup>R</sup> .	[41]
pVSP61-WspR12-Tc	pVSP61-Tc expressing the wild-type diguanylate cyclase, WspR12, Km <sup>R</sup> and Tc <sup>R</sup> .	[28, 41]
pVSP61-WspR19-Tc	pVSP61-Tc expressing the constitutively-active diguanylate cyclase mutant, WspR19 ( <i>R129C</i> ), Km <sup>R</sup> and Tc <sup>R</sup> .	[28, 41]

All plasmids were maintained in *Ec.* K12. ATCC, American Type Culture Collection. Km and Tc were used at 50 and 12.5  $\mu\text{g}\cdot\text{ml}^{-1}$ , respectively, to select for plasmids in *Ec.* K12, and at 100 and 12.5  $\mu\text{g}\cdot\text{ml}^{-1}$  for *Ba.* 197N strains, respectively. \*, Antibiotic susceptibility using MASTRING M13, M14, and M51 disks was determined for *Ba.* 197N (S, Sensitive; R, Resistant): Ampicillin (R), Cephalixin (R), Cephalthin (R), Chloramphenicol (S), Ciprofloxacin (R), Coliston sulphate (S), Cotrimoxazole (R), Erythromycin (R), Fusidic acid (R), Gentamycin (S), Nalidixic acid (R), Nitrofurantoin (R), Novobiocin (R), Oxacillin (R), Penicillin (R), Streptomycin (S), Tetracycline (S), Trimethoprim (R) (these are in agreement with [33]).

**Table 2.** Homology between *Pf.* SBW25 Wss-like bacterial cellulose synthase (Bcs) complex subunits.1  
2  
3  
4  
5  
6  
7  
8  
9  
10  
11  
12  
13  
14  
15  
16  
17  
18  
19  
20  
21  
22  
23  
24  
25  
26  
27  
28  
29  
30  
31  
32  
33

Feature	Localisation		Core synthase subunits					Acetylation-associated subunits				Localisation
	WssA	WssB	WssC	WssD	WssE	WssF	WssG	WssH	WssI	WssJ		
Reference : <i>Pseudomonas fluorescens</i> SBW25	PFLU : 0300	0301	0302	0303	0304	0305	0306	0307	0308	0309		
Length :	344	739	755	436	1279	221	221	468	374	324		
GC content :	62.7	63.0	62.0	62.8	63.2	59.8	63.1	62.4	64.5	61.1		
Compared with : <i>Bordetella avium</i> 197N	BAV : 2632	2631	2630/2629*	2628	2627	2626	2625	2624	2623	NP		
Length :	255	733	764/753	398	1323	221	222	469	389			
% Identity :	36	60	44/51	47	42	56	50	66	51			
E value :	3e-42	0	0/0	9e-116	0	3e-80	3e-52	0	5e-112			
GC content :	61.7	60.4	63.9/61.7	64.3	64.8	58.9	65.2	60.6	63.6			
<i>Pseudomonas putida</i> KT2440	PP : 2634	2635	2636	2637	2638	NP	NP	NP	NP	NP		
Length :	235	865	760	370	1172							
% Identity :	28	56	34	38	25							
E value :	0.007	0	5e-122	2e-75	3e-44							
GC content :	65.7	64.9	64.3	66.1	65.7							
<i>Pseudomonas syringae</i> DC3000	PSPTO : 1026	1027	1028	1029	1030	1031	1032	1033	1034	NP		
Length :	381	739	751	403	1230	221	224	471	383			
% Identity :	37	69	57	54	52	71	53	85	62			
E value :	5e-69	0	0	6e-147	0	9e-110	2e-66	0	2e-155			
GC content :	61.0	60.3	61.7	65.0	63.9	60.5	62.5	62.0	63.8			

The following features of the proteins listed are: genome coding sequence (PFLU, BAV, PPU and PSPTO), protein length (amino acids), BLAST % amino-acid identity and E values compared to the *Pf.* SBW25 protein, and GC content of the gene. \*, *Ba.* 197N has a duplication of *wssC* which is annotated as *wssC2* (BAV2630) and *wssC1* (BAV2629). NP, No homologue present in that gene cluster / operon.

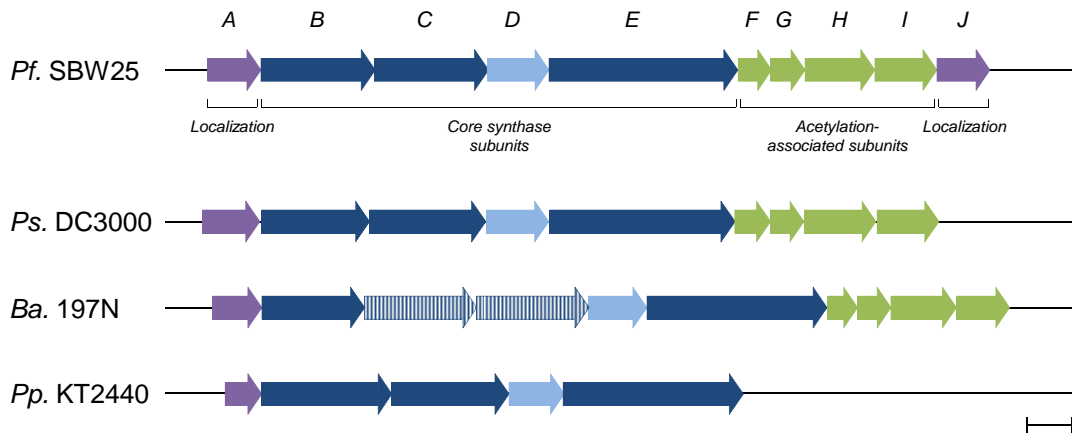


Figure 1

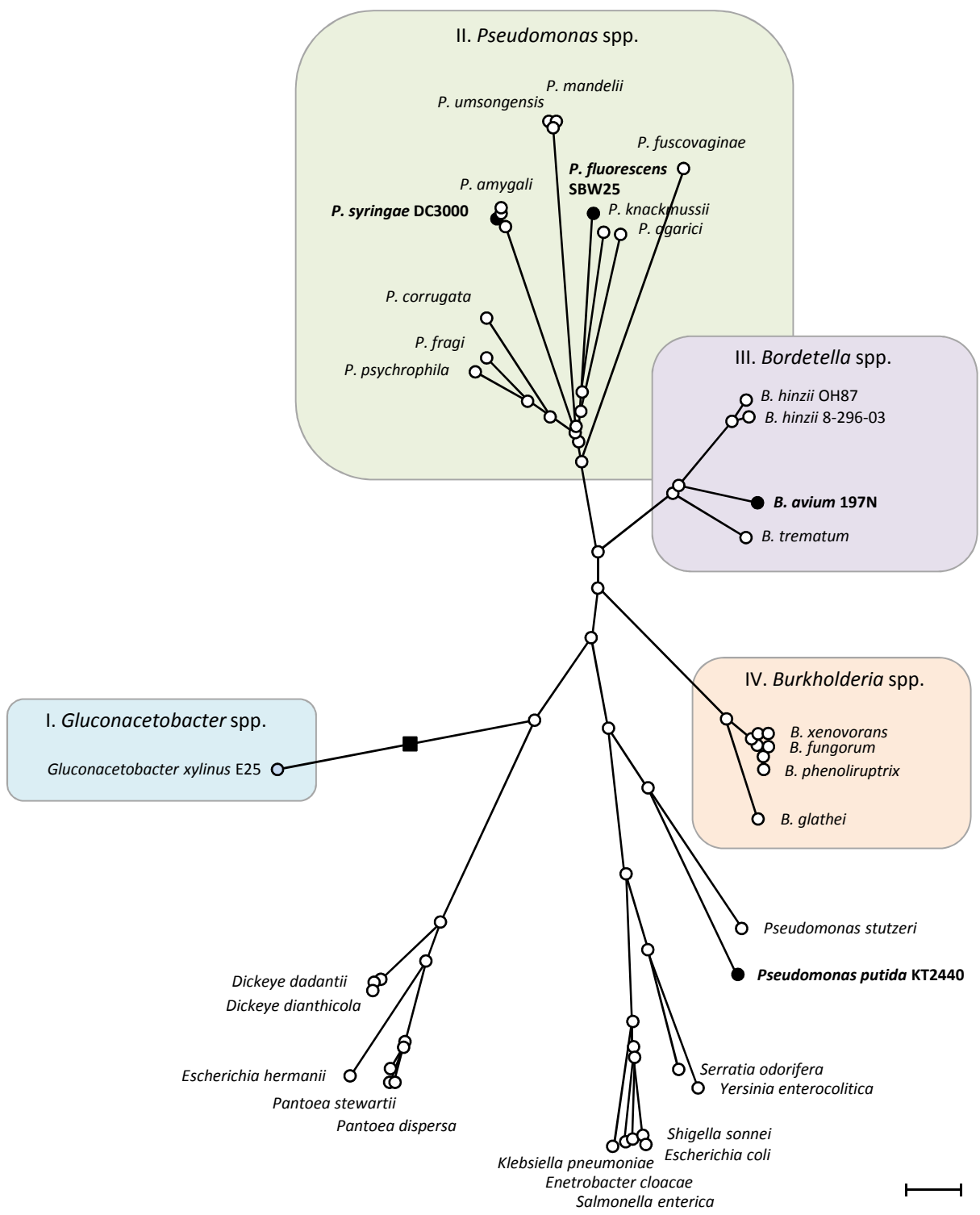


Figure 2

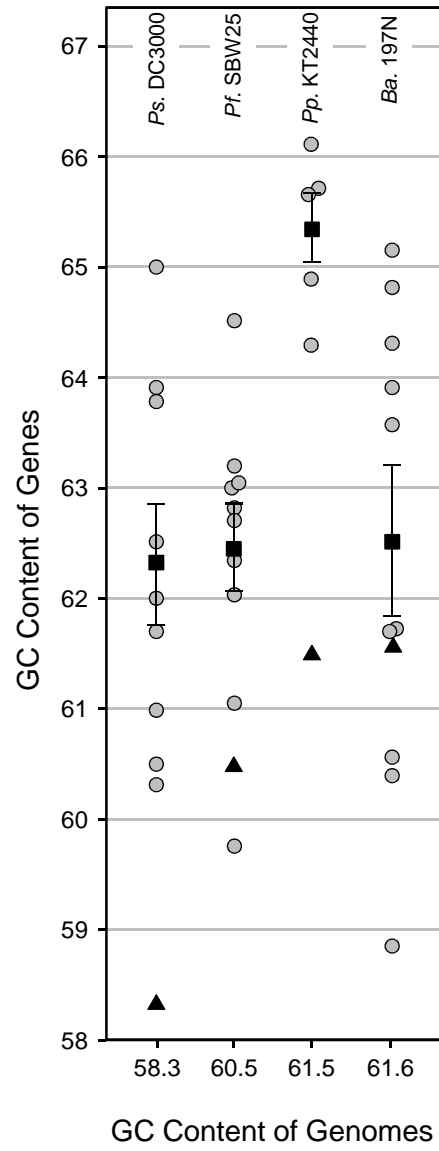


Figure 3

(A) BHI microcosms

(B) KB microcosms

(C) LB microcosms

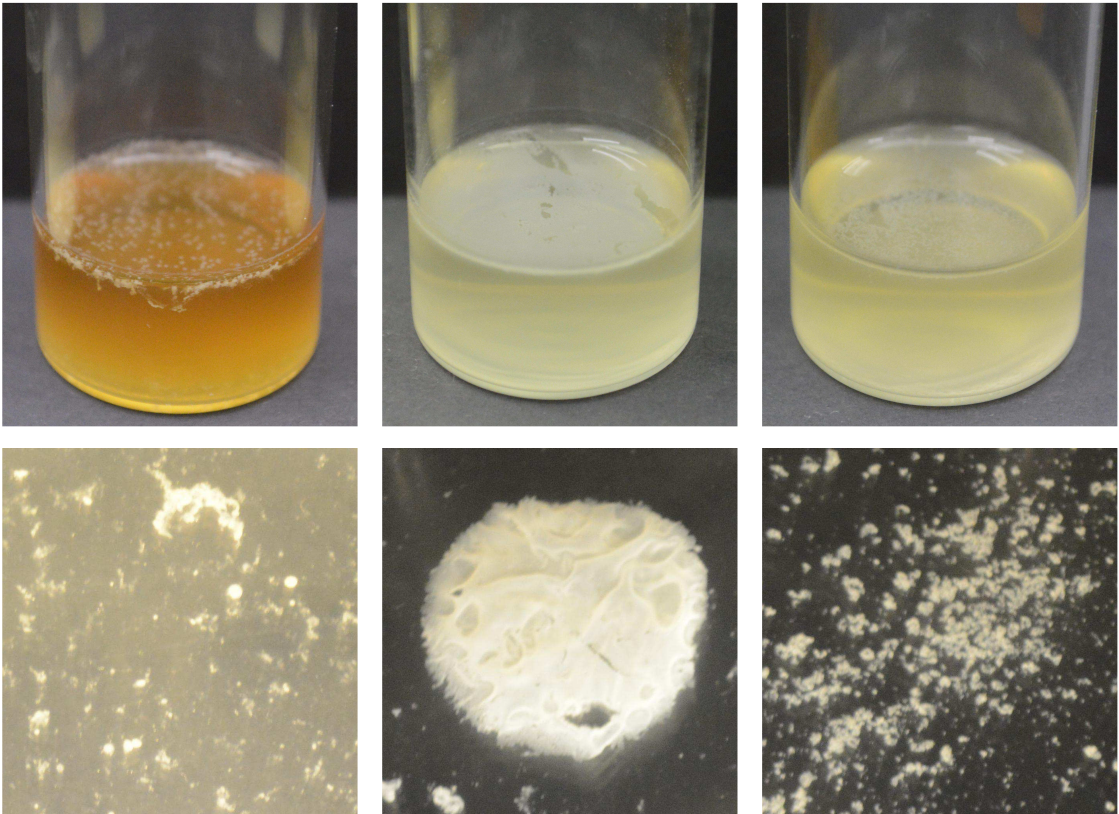


Figure 4



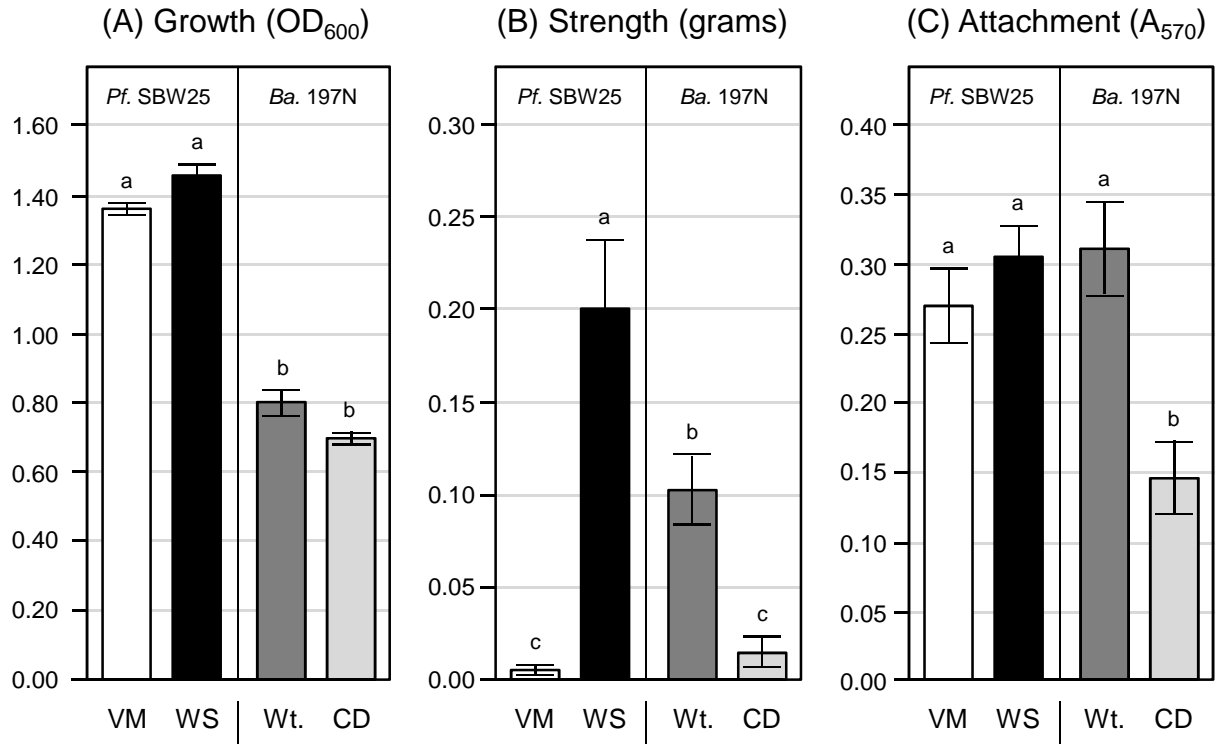
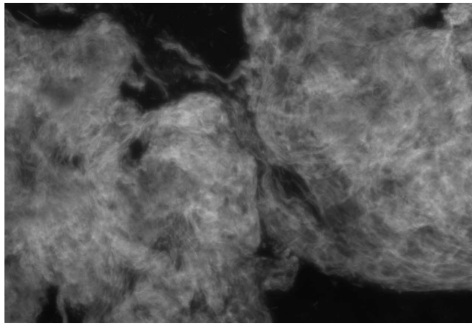
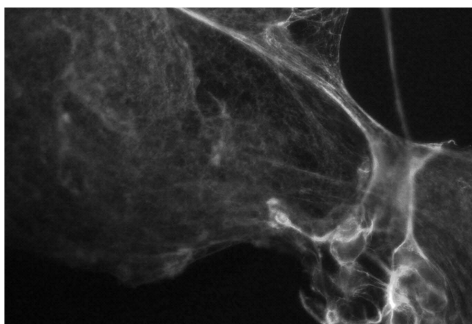


Figure 5

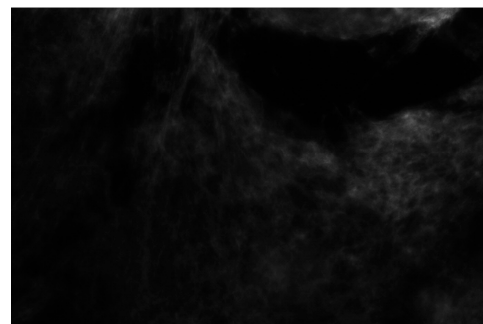
**(A) Fluorescent microscopy**



*Pf.* SBW25 Wrinkly Spreader (10x)

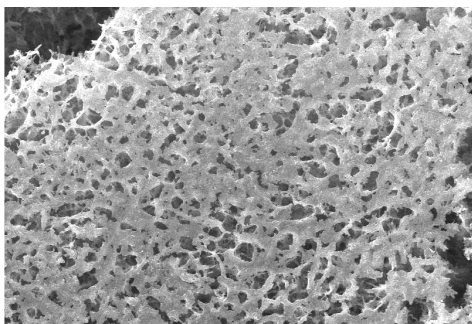


*Ba.* 197N (40x)

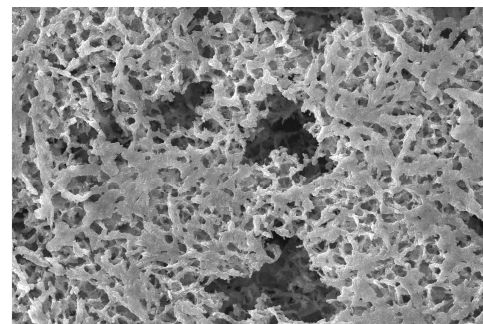


CD mutant (40x)

**(B) Scanning electron microscopy**



*Ba.* 197N (500x)



CD mutant (500x)

**(C) Congo red plates**



*Ba.* 197N

pVSP61

WspR9

WspR12

WspR19

CD

Figure 6